An Enhanced Axial-flux Magnetic-geared Machine with Dual-winding Design for Electric Vehicle Applications

Weinong Fu, Qinying Wu, Shuangxia Niu, *Senior Member*, *IEEE*, Yuanxi Chen, *Student Member*, *IEEE*, Xinhua Guo, *Senior Member*, *IEEE*

***Abstract*—Axial-flux magnetic-geared machine (MGM) is a promising solution for electric vehicle applications for combining the virtues of both axial-flux electric machine and magnetic gear. However, generalized MGMs are limited by the torque density issue, accordingly inapplicable to industrial applications. To solve the abovementioned issue, an improved axial-flux magnetic-geared machine with a dual-winding design is proposed. The key merit of the proposed design is to achieve enhanced torque performance and space utilization with the proposed design, which installs a set of auxiliary winding between modulation rings. With the proposed design, overload protection capability, and fault-tolerant capability can be also achieved, for the proposed machine can work with either the excitation of armature windings or auxiliary windings. The pole-pair, slot combination, and parametric design is studied and optimized by the 3d finite-element method and designed C++ optimization software. Electromagnetic analysis and performance comparison indicate that the proposed machine can achieve a torque enhancement of 68.6% compared to the comparison machine.**

***Index Terms*—Axial-flux, Dual-winding, Magnetic-geared machine, Torque enhancement.**

I. Introduction

ELECTRIC vehicles (EV) have emerged as one of the most promising solutions for advancing green energy and a popular research topic in recent years. The electric machines that power EVs play a critical role and must exhibit high efficiency, torque density, and reliability [1]-[3] to meet the demands of modern transportation. In the realm of EV driving systems, two general solutions have gained widespread adoption. The first type comprises a high-speed, low-torque motor, paired with a mechanical gearbox. The second type, on the other hand, employs a large-torque, low-speed direct-drive motor. Both solutions, however, come with inherent drawbacks. The former is constrained by high transmission loss, potential overload damage, considerable weight, and loud noise while the latter is limited by its inefficient performance at low operating speeds and bulky size. The Axial-flux magnetic-geared machine (AMGM) combines the benefits of two solutions, resulting in outstanding advantages such as high transmission efficiency, inherent overload protection, improved heat dissipation, and low operational noise [4]-[7]. Due to these features, the AMGM is a highly promising solution for EV applications [8]-[19]. Reference [14] investigated the potential use of the space between modulators by installing windings. However, the windings were utilized solely as an armature winding and the structure featured only one set of winding. Thus, the potential synergy between the windings remains unexplored. References [15]-[16] investigate the advantages of the axial-flux single-stator dual-rotor machine, demonstrating the effectiveness of the proposed design. These studies provide a fundamental understanding of the superiority of this design. In contrast, References [17]-[18] focus on the elimination of the modulator and the reuse of the stator core, resulting in a highly efficient use of space. These studies show the potential for significant gains in efficiency and performance by optimizing the design of the machine. Reference [19] proposed an innovative approach by placing the machine in the bore of the axial flux magnetic gear, resulting in improved space utilization within the system. However, while this structure has advantages, it lacks fault-tolerant capabilities, and the output torque is limited due to the use of a single output rotor. Besides, the yokeless and segmented armature (YASA) machine is a typical axial-flux machine with high performance. However, compared to the proposed machine, torque performance of the conventional [20] YASA machine is weaker without flux modulation effect.

To solve the abovementioned issues, this paper presents a novel dual-winding axial-flux magnetic-geared machine for electric vehicle applications. Compared to conventional designs, the proposed structure offers three key advantages.

Manuscript received March 30, 2023; revised June 25, 2023; accepted August 01, 2023. Date of publication September 25, 2023; date of current version September 18, 2023.

This work was supported by the National Natural Science Foundation of China (Grant No. 52277049); by part of the Industry-university-research Cooperation Project in Fujian Province University and Enterprise (Grant No. 2022H6026); the National Key Research and Develop Plan, Special Project of "New Energy Vehicles" (Grant No. 2022YFB2502802-2-1). (*Corresponding Author*: *Yuanxi Chen, Xinhua Guo*)

Xinhua Guo and Qinying Wu is with the college of information science and engineering, Huaqiao University, Xiamen, Fujian, 361021, China. (email: guoxinhua@hqu.edu.cn and 852932065@qq.com)

Yuanxi Chen and Shuangxia Niu is with The Hong Kong Polytechnic University, Hong Kong, 999077, China. (e-mail: 19109864r@connect.polyu.edu.hk and eesxniu@polyu.edu.hk).

Weinong Fu is with the Shenzhen Institute of Advanced Technology, Chinese Academy of Sciences, Shenzhen, 518055, China. (e-mail: wn.fu@siat.ac.cn).

Digital Object Identifier 10.30941/CESTEMS.2023.00047

1) The use of an auxiliary winding strengthens the magnetic field generated by the armature winding, resulting in a significant improvement in both output torque and overload protection capability.

2) The proposed structure inherently possesses fault-tolerant capabilities, as it can operate with either the excitation of armature windings or auxiliary windings.

3) The shared stator structure and the wing winding reduce the length of the end region, which reduces the consumption of copper and the overall weight of the machine.

II. Machine Configuration and Operating Principle Analysis

A. Machine Configuration and Parameter Study

The overall structure of the proposed machine is shown in Fig. 1(a) while the parameters and the 2D cross-section at average diameter are shown in Fig. 1(b), which consists of two rotors, two modulators, armature winding, auxiliary winding, and a shared stator. the rotors are connected with the same operating speed, while the PMs installed in the corresponding position of the two rotors have oppositely magnetized orientations shown in Fig. 2(b). Excepting the fixed axial length L_m, all the parameter combinations shown in Fig. 2(b) will be used to optimize the proposed machine.

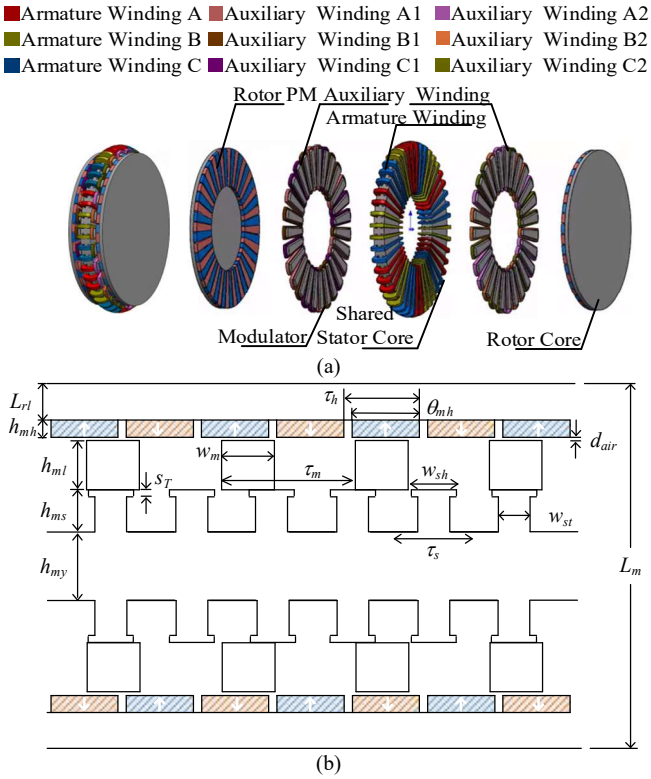

Fig. 1. Structure configuration of the proposed machine (a) 3-D and exploded view. (b) 2-D cross-section at average diameter and parameters.

The phase coils of both the auxiliary and armature windings are connected in series and utilize centralized winding. The winding electromotive force (EMF) phasors are depicted in Fig. 2(a) and 2(b). The armature winding has 45 slots, while the auxiliary winding has 27 slots. To construct a three-phase winding, 27 modulators are chosen. The wing winding is desi-

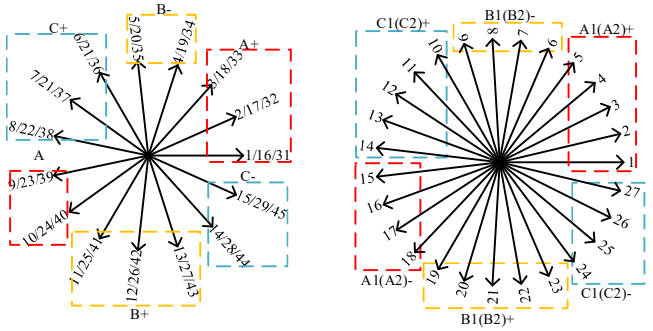

Fig. 2. Structure configuration of the proposed machine (a) 3-D and exploded view. (b) 2-D cross-section at average diameter and parameters.

gned to suit the dual-rotor structure, resulting in reduced end region length and overall machine weight.

The coil electromotive force (EMF) phasors for the proposed machine are depicted in Fig. 2, with (a) representing the armature winding and (b) representing the auxiliary winding. The driving system configuration for the proposed machine is illustrated in Fig. 3, comprising two sets of three-phase inverters and a DC source. As depicted, the corresponding auxiliary windings installed in the two sets of modulators are connected in series and operate independently of the armature winding. This sets it apart from a six-phase electric machine. This unique feature allows the proposed machine to operate with either the auxiliary winding or the armature winding excitation, providing inherent fault-tolerant capability.

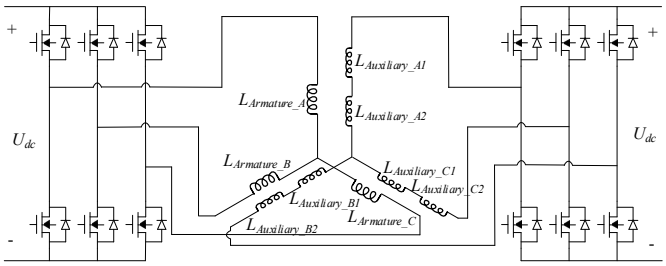

Fig. 3. Configuration of the driving system for the proposed machine.

B. Operating Principle Analysis,

The number of pole-pairs of the PMs, armature winding, and modulators of the magnetic-geared machine should follow the following rules.

$$p_1 = p_2 \pm p_3 \tag{1}$$

$$p_1\omega_1 = p_2\omega_2 \pm p_3\omega_3 \tag{2}$$

where p_1, p_2, p_3, ω_1, ω_2, and ω_3 are the pole pair and speed of armature winding, modulator, and rotor PMs.

Considering the torque density, the pole pairs of modulators should equal the summation of that of armature winding and rotor PMs [12]. Hence, the flux frequency of the armature winding and auxiliary winding under the rotation speed ω is expressed as.

$$\begin{cases} f_{\text{arm}} = -\dfrac{p_2\omega_1}{p_3 2\pi} \\ f_{\text{aux}} = -\dfrac{\omega_1}{2\pi} \end{cases} \tag{3}$$

where the f_{arm} and f_{aux} are the flux frequency of armature winding and auxiliary winding, respectively. The relationships of flux between rotor PMs, armature winding, and auxiliary winding is shown in Fig. 4.

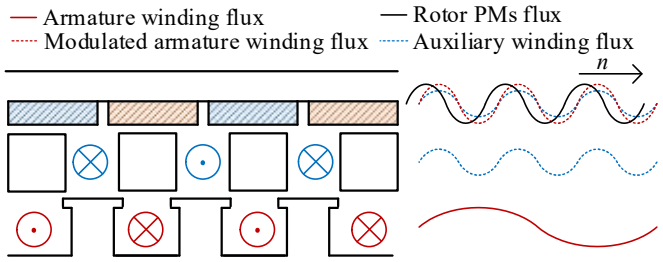

Fig. 4. The flux relationships between rotor PMs, armature winding, and auxiliary winding.

As shown in Fig. 4, the flux generated by auxiliary winding is in phase with that modulated flux of armature winding. The synthesis flux leads to the degree of flux generated by rotor PMs, making the proposed machine operates as a motor.

III. Optimization and Comparison

In this section, the genetic algorithm (GA) is utilized to optimize the performance of the proposed machine and comparison models. The GA is implemented through a co-simulation between the finite-element method (FEM) and custom-designed C++ software [21]. To optimize the machine, we use the parameters shown in Fig.1 (b). The optimized targets are selected based on multiple criteria, including output torque, ripples, and torque density, with the aim of achieving the best possible performance for the proposed structure.

A. Optimization Algorithm

The optimization procedure of the proposed machine is shown in Fig. 5 and the process is as follows.

1) The optimization process begins by setting the output torque and ripples as the targets while considering the computing power, a population quantity of 100 is selected.

2) Next, models with varying parameters are generated, selected, and calculated. The parameter combination that delivers superior performance is saved for use in the optimization of the next generation. If a combination fails to meet performance criteria, it is discarded to conserve computational resources [22]-[25].

3) To ensure that computational resources are used efficiently, the calculated models are subjected to qualification checks, preventing the computer from wasting resources on models with unreasonable dimensional parameters.

4) Finally, the optimization process concludes once the iterations reach the pre-defined setpoint, which in this design is 100. By employing co-simulation, the optimization process can effectively design an optimized structure.

The parameter range of the optimization parameters and fixed parameters of the proposed machine is shown in Tables I and II. The fixed parameters include the air gap length, current density, and pole-pair numbers, to ensure that the optimization is conducted in a fixed topology [26]-[30].

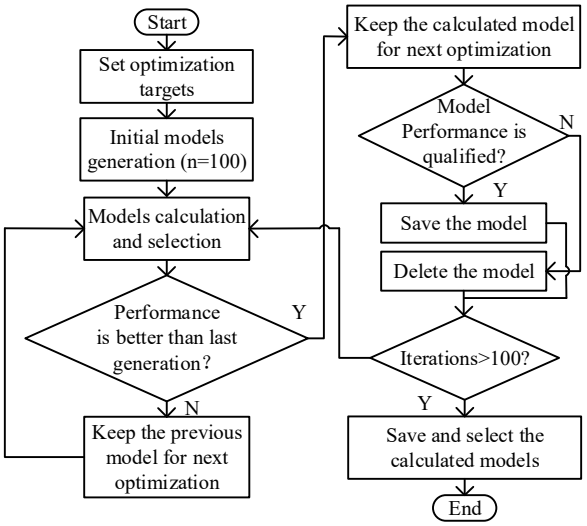

Fig. 5. Designed optimization procedure of the proposed machine.

TABLE I
FIXED PARAMETERS

Symbol	Quantity	Value
N_S	Number of slots	45
N_m	Number of modulators	27
N_{pm}	Pole-pairs of PM	24
L_m	Axial-length of machine	60mm
D_o	Outer diameter of stator/modulator	92mm
D_i	Inner diameter of stator/modulator	46mm
d_{air}	Air gape	0.5mm
K_s	Slot package factor	0.6
J	Rated current density	6A/mm^2
ω	Nominal speed	300rpm

TABLE II
OPTIMIZED PARAMETERS

Symbol	Quantity	Range	Optimized Results
θ_{mh}/τ_h	Rotor magnetic angle ratio	0.8-1	0.95
w_m/τ_m	Modulator angle ratio	0.7-1.3	1.1
w_{sh}/τ_s	Pole shoe angle ratio	0.5-0.8	0.72
w_{st}/τ_s	Stator tooth angle ratio	0.4-0.7	0.68
L_{rl}	Rotor yoke thickness	2-6 mm	4.5
h_{mh}	Rotor PM thickness	1.5-4 mm	3.05
h_{ml}	Modulator thickness	2.5-6 mm	7.97
s_T	Pole shoe thickness	0.5-1 mm	0.98
h_{ms}	Stator tooth thickness	3-7 mm	6.9
h_{my}	Stator yoke thickness	5-13 mm	11.2

B. Optimization Result Comparison

The optimized parameters of the proposed machine are given in Table II and the corresponding performance of the proposed machine under different parameter combinations is given in Fig. 6, indicating the relationship between torque, torque ripple, and torque density versus PM consumption as well as the optimized solution region. As shown in Fig. 6, the optimized solution of the proposed machine can achieve a maximum output torque of 167.38 N·m and torque density of 0.87N·m/cm^3 versus PM consumption with a ripple of 0.044.

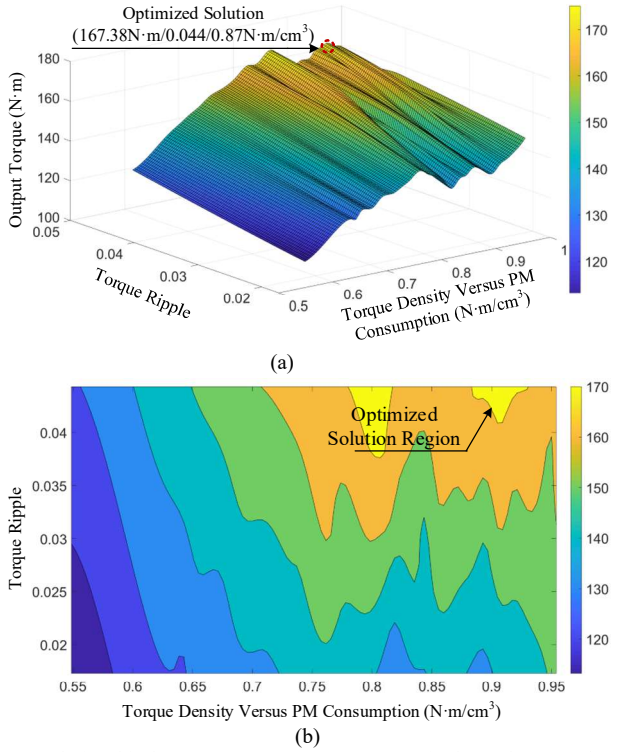

Fig. 6. Relationship between output torque, torque ripple, and torque density versus PM comsumption. (a) 3D surface. (b) 2D figure under xy plane.

To conduct a fair comparison, the proposed machine and comparison models, including the axial-flux dual-rotor magnetic-geared machine (model I), axial-flux permanent magnet machine (model II), dual-winding single-rotor axial-flux generalized magnetic-geared machine, (model III), and axial magnetic-geared machine (model IV), will be optimized. The topology of comparison models is given in Fig. 7. Those comparison models have the same volume, current density, and material as the proposed machine. Excepting the generalized PM and magnetic-geared machine (model II and III), model I has the same shared stator topology with the proposed machine while model III has the same dual-winding topology with the proposed machine.

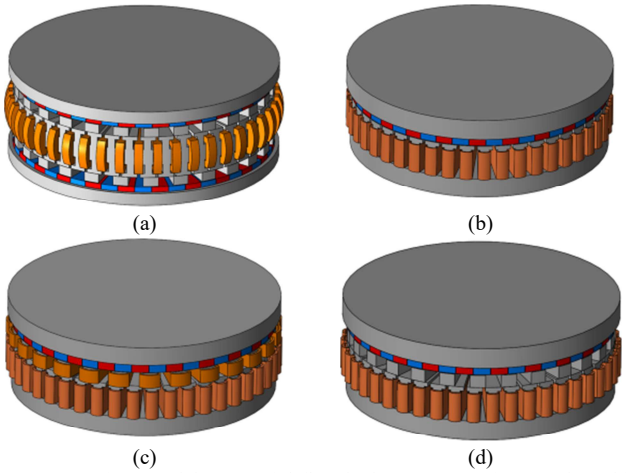

Fig. 7. Comparison models. (a) Axial-flux dual-rotor magnetic-geared machine (model I). (b) Axial-flux permanent magnet machine (model II). (c) Dual-winding single rotor axial-flux generalized magnetic-geared machine (model III). (d) Axial magnetic-geared machine (model IV).

As shown in Fig. 8, the comparison models all have poor performance compared to the proposed machine. The maximum output torque of models I, II, III, and IV only reaches 99.2, 106.4, 149.5, and 97.24, respectively. Based on the optimized solutions conducted in this section, a comprehensive comparison between the proposed machine and comparison models will be conducted in section IV.

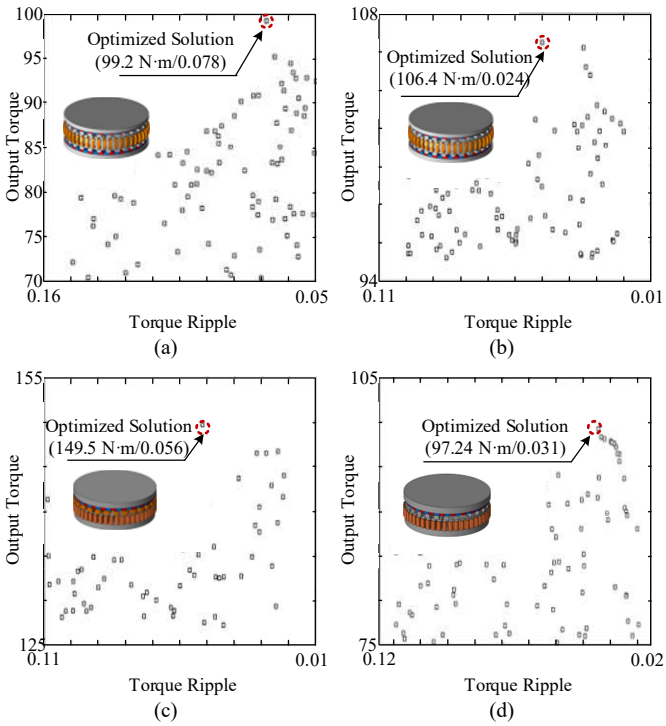

Fig. 8. Optimization results of comparison models. (a) Axial-flux dual-rotor magnetic-geared machine (model I). (b) Axial-flux permanent magnet machine (model II). (c) Dual-winding single rotor axial-flux generalized magnetic-geared machine (model III). (d) Axial magnetic-geared machine (model IV).

IV. Performance Analysis and Comparison

A. Slot Combination Investigation and Comparison

The pole pair of the stator, modulation rings and rotor permanent magnets (PMs) are fixed. The impact of slot number on back EMF is investigated and given in Fig. 9, with slot numbers 36, 45, and 54.

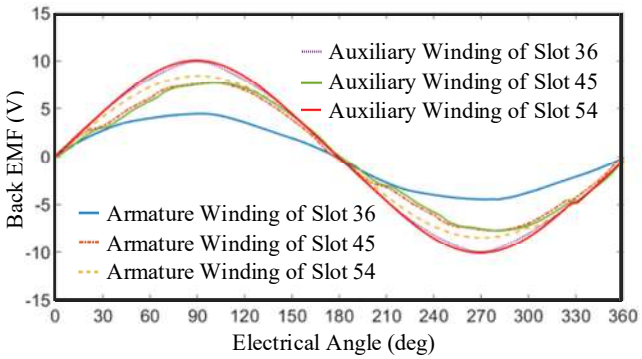

Fig. 9. Back EMF of winding with different number of slots.

The results given in Fig. 9 indicate that, under no-load conditions, the proposed machine with the armature winding

and auxiliary winding of 36, 45, and 54 slots exhibits peak back EMF values of 4.46V, 7.69V, and 8.41V, as well as 9.96V, 7.68V, and 10.06V.

Fig. 10 shows the results of the fast Fourier transform (FFT), indicating that the total harmonic distortion (THD) contents of the armature winding's back EMF are 3.91%, 5.71%, and 0.21%, while those of the auxiliary winding are 3.06%, 2.60%, and 3.38%. Those results reveal that there is not a significant difference in the harmonic distortion rates of the back EMF in both windings. Although the proposed machine with 54 slots and 36 slots has the highest peak value in the armature and auxiliary winding, respectively (as shown in Fig. 9), the volume of inverter required for the normal operation would be larger, resulting in increased manufacturing costs. Therefore, the THD is not the most important consideration for determining the combination. In this paper, the 45-slot combination is chosen considering the abovementioned issues.

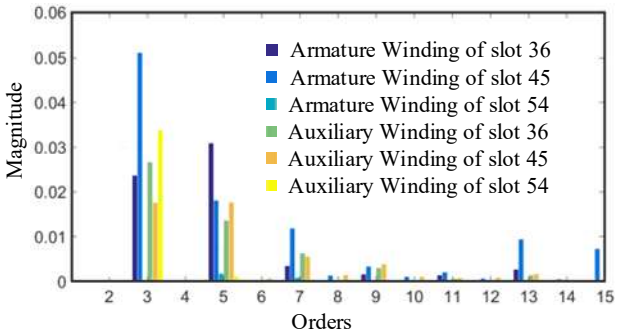

Fig. 10. FFT of back EMF of winding with different number of slots.

The Back EMF waveforms of the armature and auxiliary windings for motor I, II, III, and IV are depicted in Fig. 11. Additionally, the FFT analysis reveals the THD for each winding of motor I, II, III, and IV, as shown in Fig. 12.

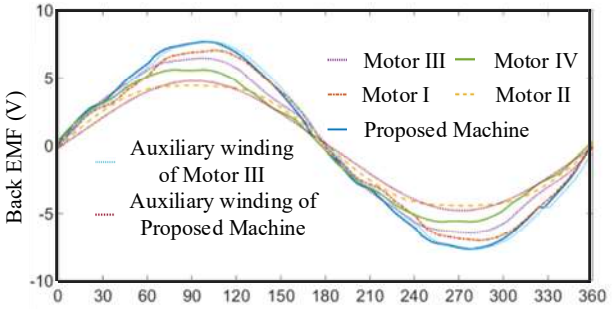

Fig. 11. Back EMF of the proposed machine, motor I, II, III and IV.

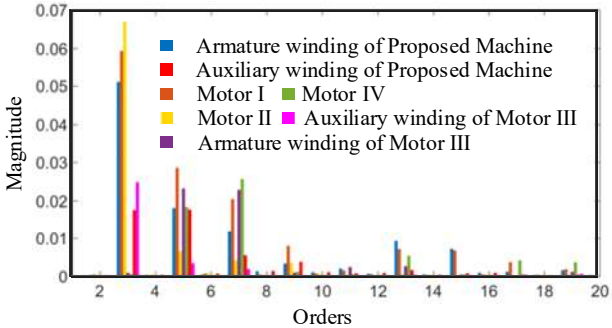

Fig. 12. FFT of back EMF of the proposed machine, motor I, II, III and IV.

The THD for the armature winding and auxiliary winding of the proposed machine are 5.71% and 2.42%, respectively. For motor I, II, and IV, the corresponding THD are 7.05%, 6.76%, and 3.25%, respectively. Besides, the THD values for the armature winding and auxiliary winding of Motor III are 3.28% and 2.52%, respectively.

B. Finite Element Analysis and Efficiency Comparison

The Finite element analysis (FEA) of the proposed machine under no-load and full-load conditions are given as Fig. 13. Under the full-load condition, the current density of the armature winding and auxiliary winding are both 6A/mm^2. As indicated in Fig. 13, the magnetic induction intensity of the proposed machine is lower than 1.8T under the full-load condition, which is less prone to saturation.

The efficiency map of the proposed machine as well as comparison motors I, II, III, and IV is given in Fig. 14. The

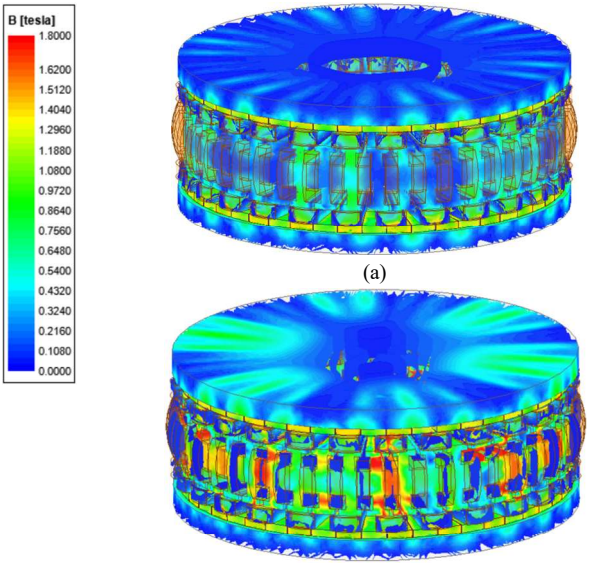

Fig. 13. FEA results of the proposed machine under different operating conditions. (a) no-load condition. (b) full-load condition.

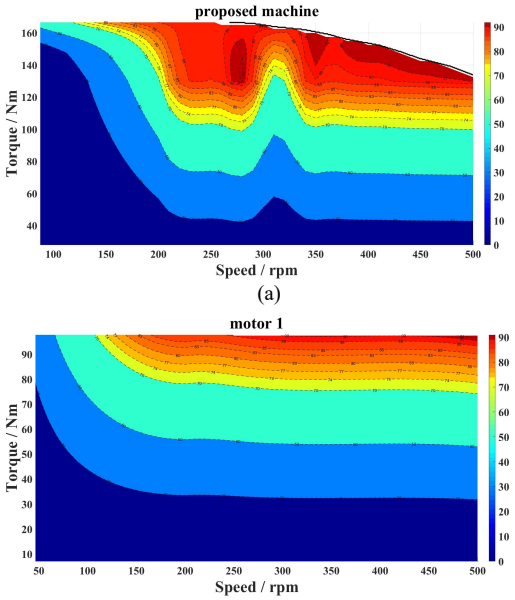

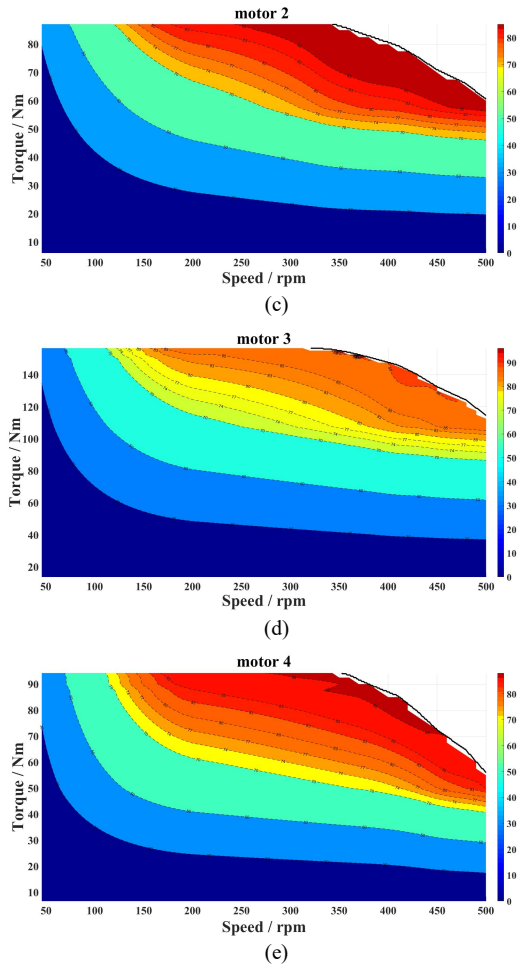

Fig. 14. Efficiency map of the proposed machine and motor I, II, III, and IV. (a) The proposed machine. (b) Motor I. (c) Motor II. (d) Motor III. (e) Motor IV.

efficiency of the proposed machine can reach 90% under rated conditions.

Apart from the efficiency map given in Fig. 14, the comprehensive comparison of the proposed machine and comparison machine is given in part C, including the efficiency, power factor, torque performance, overload capability, and torque density.

C. *Torque Performance Investigation*

The cogging torques of the proposed machine, motor I, II, III, and IV are shown in Fig. 15. The proposed machine has nearly the smallest cogging torque compared with comparison models. The torque performance of those machines is given in Fig. 16.

As shown in Fig. 15, the cogging torques of those machines only reach a maximum of 1.19%, 2.02%, 1.88%, 2.54%, and 4.12% of their full load torque capacity. Besides, the proposed machine outperforms them all in terms of the cogging torque to full load torque ratio. Additionally, the proposed machine exhibits exceptional torque performance, as illustrated in Fig. 16. It boasts the best torque output capacity, with a 68.6% increase compared to motor I, 57.5% compared to motor II, 6.4% compared to motor III, and a staggering 72.16% compared to motor IV. Its peak torque output is an impressive 167.13 N·m, with a ripple of 7.38%. For a comprehensive overview of the comparison results, refer to Table III. Notably, the proposed machine exhibits the highest efficiency and torque density. The power factor of the proposed machine and comparison models are provided in Table III.

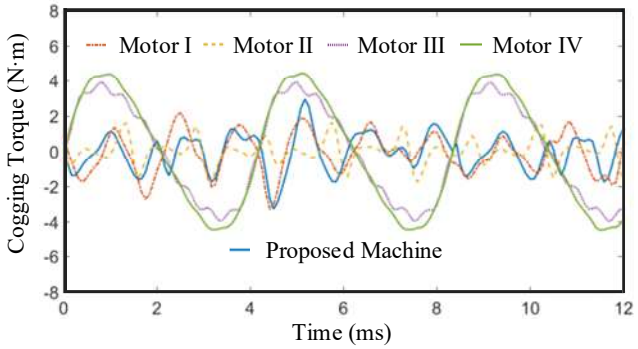

Fig. 15. Cogging torque of the proposed machine, Motor I, II, III and IV.

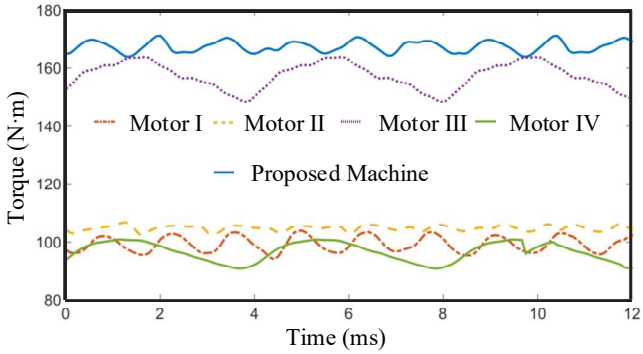

Fig. 16. Rated torque of the proposed machine, Motor I, II, III and IV.

TABLE III
COMPREHENSIVE COMPARISON RESULT

	This Paper	Motor II	Motor II	Motor III	Motor IV
Efficiency (%)	91.73	91.57	88.12	88.40	89.41
Toque density (N·m/kg)	12.07	9.63	7.71	10.24	8.70
Toque density Per PM (N·m/kg)	153.36	97.53	59.36	192.4	90.47
Output torque (N·m)	166.13	99.34	106.2	157.5	97.83
Copper loss (W)	336.06	151.2	368.7	539.0	302.5
Core loss (W)	75.68	99.22	80.12	108.8	58.98
Weight (kg)	13.83	10.30	13.74	15.32	11.14
Power Factor (Armature winding)	0.705	0.913	0.94	0.684	0.891
Power Factor (Auxiliary winding)	0.891	N.A.	N.A.	0.967	N.A.

D. *Overload and Efficiency Analysis*

Fig. 17 displays the overload capacity of the proposed machines, depicting their torque performance as the current density increases from 2 A/mm^2 to 20 A/mm^2.

The proposed machine indicates the best overload capacity compared to motor I, II, III, and IV. The proposed machine can improve the output torque from 65.2 N·m at 2 A/mm^2 to 292 N·m at 20 A/mm^2. While it may not have an advantage in relative torque density compared to motor III at a current density of 6 A/mm^2, the proposed machine does significantly alleviate the saturation problem of motor III. The efficiency comparison of the proposed machine and motor I, II, III, and IV is depicted in Fig. 18.

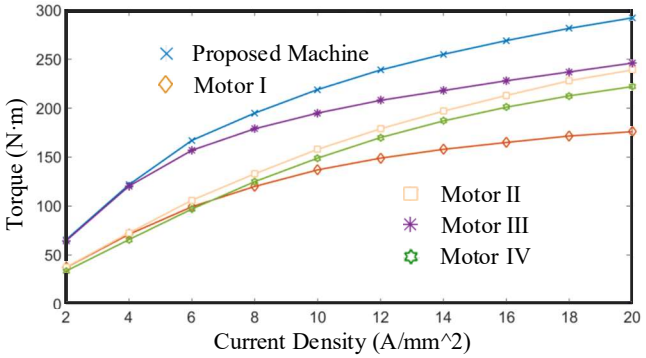

Fig. 17. Output torque versus current density.

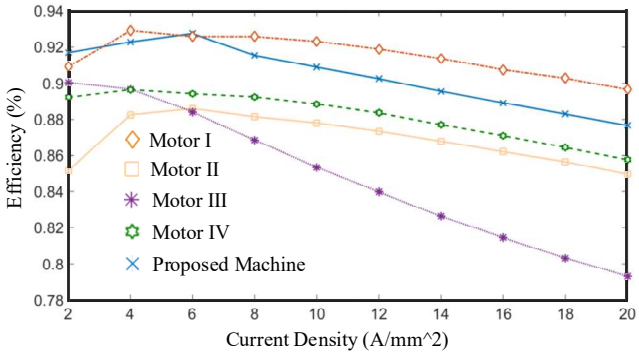

Fig. 18. Output torque versus current density.

Based on the results presented in Fig. 18, the proposed machine achieves maximum efficiency at a current density of 6A/mm2, with a peak value of 92.73%. Although Motor I exhibits the highest efficiency in most cases, it falls short in terms of torque density compared to the proposed machine. In summary, the proposed machine has a comparative advantage over the other machines in terms of torque density, efficiency, and overload capacity.

Fig. 19 investigates the potential of the fault tolerance capability of the proposed machine, as it can operate with the excitation of either the armature winding or the auxiliary winding. To conduct a fair comparison, the proposed machine is compared to model III, which also has two sets of windings.

Results in Fig. 19 indicate that the proposed machine can function normally with only the excitation of the armature winding, at a current density of 16 A/mm^2, or with only the excitation of the auxiliary winding, at a current density of nearly 10 A/mm^2. This is a significant advantage not available to other types of axial-flux magnetic-geared machines. Additionally, compared to model III, the proposed machine exhibits a better torque output capacity under fault conditions at the same current density.

V. Conclusion

This paper proposes an enhanced axial-flux magnetic-geared machine with dual-winding design for electric vehicle applications. Firstly, the paper introduces the machine's structure, corresponding coil-emf vectors, and working principle. Next, the paper conducts a performance comparison of the proposed machine with different slot numbers to determine the optimal design. Additionally, the paper conducts a quantitative comparison of the proposed machine's perform-

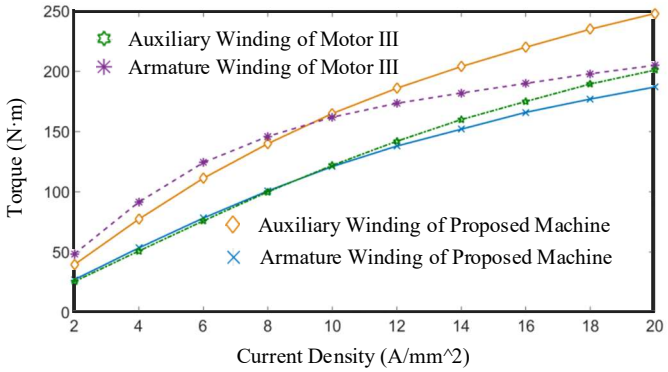

Fig. 19. Output torque versus current density with sole excitation of armature winding or auxiliary winding.

ance against other machines, including axial-flux magnetic-geared machine, axial-flux PM machine, dual-winding axial-flux magnetic-geared machine with single modulator, and axial-flux magnetic-geared machine with a single modulator. The comparison results indicate that the proposed machine has a significant advantage in torque density (12.07 N·m/kg), efficiency (92.73%), overload capacity, and potential fault-tolerance capacity, thus making it a potential solution choice for electric vehicle applications.

References

[1] W. N. Fu, and L. Li, "Optimal Design of Magnetic Gears with a General Pattern of Permanent Magnet Arrangement," *IEEE Trans*. Appl. Supercond., vol. 26, no. 7, pp. 1-5, Oct. 2016.

[2] S. Niu, N. Chen, and S. L. Ho *et al*, "Design Optimization of Magnetic Gears Using Mesh Adjustable Finite-element Algorithm for Improved Torque," *IEEE Trans. Magn*., vol.48, no.11, pp. 4156-4159, Nov, 2012.

[3] Y. Liu, S. L. Ho and W. N. Fu, "A Novel Magnetic Gear with Intersecting Axes," *IEEE Trans. Magn*., vol. 50, no.11, pp.1-4, Nov, 2014.

[4] Q. Wang, S. Niu, and S. Yang, "Design Optimization and Comparative Study of Novel Magnetic-Geared Permanent Magnet Machines," *IEEE Trans. Magn*., vol. 53, no. 6, pp. 1-4, June 2017.

[5] L. Jian, K. T. Chau, and J. Z. Jiang, "A Magnetic-geared Outer-rotor Permanent-magnet Brushless Machine for Wind Power Generation," *IEEE Trans. Ind. Appl*., vol. 45, no. 3, pp. 954-962, May, 2009.

[6] X. Zhang, X. Liu, and Z. Chen, "A Novel Coaxial Magnetic Gear and Its Integration with Permanent-magnet Brushless Motor," *IEEE Trans. Magn*., vol. 52, no. 7, pp. 1-4, July, 2016.

[7] L. Sun, M. Cheng, and J. Zhang *et al*, "Analysis and Control of Complementary Magnetic-geared Dual-rotor Motor." *IEEE Trans. Ind. Electron.*, vol. 63, no. 11, pp. 6715-6725, Nov. 2016

[8] C. Liu, K. T. Chau, and J. Zhong *et al*, "Quantitative Comparison of Double-stator Permanent Magnet Vernier Machines with and Without HTS Bulks," *IEEE Trans. Appl. Supercond*., vol. 22, no. 3, pp. 5202405-5202405, June 2012.

[9] M. Johnson, M. C. Gardner, and H. A. Toliyat, "Design and Analysis of 11an Axial Flux Magnetically Geared Generator," *IEEE Trans. Ind. Appl*., vol. 53, no. 1, pp. 97-105, Jan.-Feb. 2017.

[10] H. Lin, S. Niu, and Y. Chen *et al*, "Three-Stage Duty Cycle-based Deadbeat Predictive Torque Control for Three-phase SPMSMs With CMV Reduction" *IEEE Transactions on Power Electronics*, early access, doi: 10.1109/TPEL.2023.3288184.

[11] H. Lin, S. Niu, and Z. Xue, *et al*, "A Simplified Virtual-vector-based Model Predictive Control Technique with a Control Factor for Three-phase SPMSM Drives," *IEEE Transactions on Power Electronics*, vol. 38, no. 6, pp. 7546-7557, June 2023.

[12] M. B. Kouhshahi, J. Z. Bird, and V. M. Acharya *et al*, "An Axial Flux Focusing Magnetically Geared Generator for Low Input Speed

Applications." *IEEE Trans. on Ind. Appl.*, vol. 56, no. 1, pp. 138-147, Jan. 2020.

[13] S. L. Ho, S. Niu, and W. N. Fu, "Design and Analysis of a Novel Axial-flux Electric Machine," *IEEE Trans. Magn*., vol. 47, no. 10, pp. 4368-4371, Oct, 2011.

[14] S. Gerber and R. -J. Wang, "Cogging Torque Definitions for Magnetic Gears and Magnetically Geared Electrical Machines," *IEEE Trans. Magn*, vol. 54, no. 4, pp. 1-9, April 2018.

[15] K. Y. Hwang, S. I. Kim, and B. K. Song, "Single Winding Type Determination of Dual Winding Three-phase Motor Considering Overheat Problem in Integrated Electric Braking System of Autonomous Vehicles," *IEEE Trans. Transport. Electrific.,* vol. 9, no. 1, pp. 656-666, March 2023.

[16] G. Liu, P. Zheng, and J. Bai, J. Liu *et al*, "Investigation of a Dual-Winding Dual-Flux-Concentrated Magnetic-Field-Modulated Brushless Compound-Structure Machine," *IEEE Trans. Magn*, vol. 58, no. 2, pp. 1-5, Feb. 2022.

[17] Y. Chen, W. Fu, and *et al*, "A Torque-Enhanced Magnetic-geared Machine with Dual-series-winding and Its Design Approach for Electric Vehicle Powertrain," *Sustainability*, vol. 15, no. 6, pp. 5077-5093, Mar. 2023.

[18] Y. Chen, X. Zhao, and S. Ho, *et al*, "Design and Optimization of Yokeless Magnetic Gear with Asymmetric Halbach Permanent Magnet Array for Electric Vehicle Powertrain," *IET RENEW. POWER. GEN.*, vol. 16, no. 11, pp. 2223-2232, June. 2022.

[19] Y. Chen, X. Guo, and *et al*, "Hybrid PWM Modulation Technology Applied to Three-level Topology-based PMSMs," *J.POWER ELECTRON,* vol. 19, no. 1, pp. 146-157, Jan. 2019.

[20] X. Guo, Q. Wang, and R. Shang *et al*, "Design and Analysis of a Novel Synthetic Slot Dual-PM Machine," *IEEE Access,* vol. 7, pp. 29916-29923, Mar.2019.

[21] M. F. H. Khatab, Z. Q. Zhu, and *et al*, "Comparative Study of Novel Axial Flux Magnetically Geared and Conventional Axial Flux Permanent Magnet Machines," *CES Transactions on Electrical Machines and Systems*, vol. 2, no. 4, pp. 392-398, Dec. 2018.

[22] C. Li, X. Guo, and J .Fu *et al*, "Design and Analysis of a Novel Double-stator Double-rotor Motor Drive System for In-wheel Direct Drive of Electric Vehicles. "*Machines*. vol. 10, no. 1,pp. 27-39,Dec.2022.

[23] X. Guo, S. Wu, and W. Fu *et al*, "Control of a Dual-stator Flux-modulated Motor for Electric Vehicles. "*Energies*. vol. 9, no. 7,pp. 517-535, Jul.2016.

[24] S. Mezani, T. Hamiti, and L. Belguerras *et al*, "Magnetically Geared Induction Machines," *IEEE Trans. Magn*, vol. 51, no. 11, pp. 1-4, Nov. 2015.

[25] S. Yousefnejad, H. Heydari, and K. Akatsu *et al*, "Analysis and Design of Novel Structured High Torque Density Magnetic-geared Permanent Magnet Machine," *IEEE Access*, vol. 9, pp. 64574-64586, 2021.

[26] Y. Cao, L. Feng, and R. Mao *et al*, "Analysis of Analytical Magnetic Field and Flux Regulation Characteristics of Axial-flux Permanent Magnet Memory Machine," *IEEE Trans. Magn*, vol. 58, no. 9, pp. 1-9, Sept. 2022.

[27] A. González-Parada, F. Trillaud, and R. Guzmán-Cabrera *et al*, "Torque Ripple Reduction in an Axial Flux High Temperature Superconducting Motor," *IEEE Trans. Appl.Supercond.*, vol. 25, no. 3, pp. 1-5, June 2015.

[28] P. Jin, Y. Yuan, and J. Minyi *et al*, "3-D Analytical Magnetic Field Analysis of Axial Flux Permanent-Magnet Machine,"*IEEE Trans. Magn*, vol. 50, no. 11, pp. 1-4, Nov. 2014.

[29] M. He, W. Li, and J. Peng *et al*, "Multi-layer quasi three-dimensional equivalent model of axial-flux permanent magnet synchronous machine," *CES Trans. Electrical Machines and Systems,* vol. 5, no. 1, pp. 3-12, Mar. 2021.

[30] L. Balasubramanian, N. A. Bhuiyan, and A. Javied *et al*, "Design and Optimization of Interior Permanent Magnet (IPM) Motor for Electric Vehicle Applications," *CES Trans. Electrical Machines and Systems*, vol. 7, no. 2, pp. 202-209, June 2023.

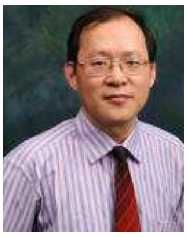

Weinong Fu received the Ph.D. degree from The Hong Kong Polytechnic University (PolyU), Hong Kong, SAR, China, in 1999.

He is currently a Professor with Shenzhen Institutes of Advanced Technology, Chinese Academy of Sciences, Beijing, China. For 13 years, he was an Associate Professor and a Full Professor with PolyU. He was a Key Developer with Ansoft Corporation, Pittsburgh, PA, USA. He has about seven years of working experience with Ansoft, focusing on the development of commercial software Maxwell. His research interests include computational electromagnetics, optimal design of electric devices, applied electromagnetics, and novel electric machines. He has made many contributions to the theory and application of electromagnetic field computation and electric device designs, including the publication of more than 250 refereed journal papers.

Qinying Wu received the B.Sc degree from Xiamen University Tan Kah Kee College, Zhangzhou, China, in 2019, She is currently working toward the M.Sc. degree in Huaqiao University, Xiamen, China.

Her research interests include motor design, oriented silicon steel materials, permanent magnet vernier motor, and drive control.

Shuangxia Niu (Senior Member, IEEE) received the B.Sc. and M.Sc. degrees from Tianjin University, Tianjin, China, and the Ph.D. degree from the University of Hong Kong, Hong Kong, SAR, China, all in electrical engineering. She is currently a Professor with the Department of Electrical and Electronic Engineering, The Hong Kong Polytechnic University. She authored or coauthored more than 100 papers in leading journals.

Prof. Niu is currently an Associate Editor for the IEEE JOURNAL OF EMERGING AND SELECTED TOPICS IN POWER ELECTRONICS.

Yuanxi Chen received the B.Eng. and M.Eng. degrees from Huaqiao University, Xiamen, China, in 2015 and 2018, respectively. He is currently working toward the Ph.D. degree in electrical engineering with The Hong Kong Polytechnic University, Hong Kong, SAR, China.

His research interests include electrical machine, electromagnetic metamaterial, transformer and wireless power transmission.

Xinhua Guo was born in Fujian, China, in 1977. He graduated from the Nanjing Institute of Technology, Nanjing, China, in 2000. He received the M.S. degree in agricultural electrifification and automation from Jiangsu University, Zhenjiang, China, in 2006, and the Ph.D. degree in electrical engineering from the Institute of Electrical Engineering (IEE), Chinese Academy of Sciences (CAS), Beijing, China, in 2010.

He is currently working as a Professor and the Deputy Dean of the College of Information Science and Engineering, Huaqiao University, Xiamen, China. In addition, he had been a Research Assistant at IEE, CAS, and worked as an Engineer at the Japanese company TDK and the American company Amphenol Assemble Tech (Xiamen) Company Ltd. His current research interests include IGBT packaging technology, PMSMs and their drive control for EVs, and special motors and their drive control. The technical achievements of his research have been industrialized through Zhejiang Semiharv Technology Company Ltd., Taizhou, China, and Xiamen Wise Electrical Technology Company Ltd., Xiamen, respectively, where he is a Technical Consultant.

Dr. Guo is also the Chairperson of Fujian Power Supply Society.